

Simulation assisted design of a gallium phosphide n–p photovoltaic junction

Charles R. Allen, Jong-Hyeok Jeon^{*}, Jerry M. Woodall

Birk Nanotechnology Center, Electrical and Computer Engineering, Purdue University, 1205 W State Street, West Lafayette, IN, USA

ARTICLE INFO

Article history:

Received 27 May 2009

Received in revised form

11 January 2010

Accepted 12 January 2010

Available online 11 February 2010

Keywords:

Gallium phosphide

Solar cell

Multi-junction

CPV

Simulation

ABSTRACT

A gallium phosphide photovoltaic junction is reported. Using a n–p structure, a gallium phosphide junction is grown on a gallium phosphide substrate by molecular beam epitaxy. Junction design is presented with measurements of the dark and light response. The light current was measured under an illumination of air mass (AM) 1.5. Without an anti-reflective coating, a V_{oc} of 1.53 V and a J_{sc} of 0.959 mA/cm² is achieved at one-sun AM1.5 global. A simulation of the junction is presented with best-fit parameters. Strategies for efficiency improvements are discussed which yield a simulated V_{oc} of 1.93 V and an AM 1.5 efficiency of 14% at 20 suns. Justification of a 51.3% efficient, ideal, multi-junction device is also presented.

© 2010 Elsevier B.V. All rights reserved.

1. Introduction

Alternative energy sources, such as solar photovoltaics, are regaining public attention. In order to reach efficiencies over 35%, solar cells must be multi-junction devices [1]. The overall efficiency of a multi-junction device depends heavily on the individual efficiencies of each junction for its portion of the spectrum. In the pursuit of higher and higher efficiencies, a suitable wide-bandgap junction must be designed that achieves maximum energy conversion efficiency in the realm of the blue-green to ultra-violet solar photons. Candidates for high-efficiency junctions were investigated, revealing gallium phosphide (GaP) as a good candidate.

GaP can be grown with diffusion lengths on the order of microns [2] on GaP substrates. Recent developments in growing III-V materials on Silicon and Germanium [3] provide a promising future for growing GaP on less expensive substrates. The band structure for GaP suggests that neither radiative recombination, nor auger recombination will be a dominating mechanism [4]. The band structure of GaP is such that the direct band edge is only 0.5 eV above the indirect band edge [5]. This yields high absorption coefficients for much of the spectrum of interest. Prior work from Sulima, et al. investigated AlGaP solar cells for space applications [6]. The ability to grow single-crystal on a GaP substrate, the ability to produce diffusion lengths on the order of microns, and the high absorption coefficients of GaP

make it a promising candidate for a wide bandgap photovoltaic material.

2. Material and methods

2.1. Device growth and fabrication

The junction is grown by MBE. A highly doped buffer layer was grown on a GaP substrate (Fig. 1). A 4.5 μm p-type active region of GaP doped 1×10^{17} with Be. This was followed by a 0.5 μm n-type active region of GaP doped 1×10^{18} with Si. The structure was capped with a heavily doped 100 Å contact layer. No anti reflection (AR) coating was used at this stage.

An annealed Au/Ge/Ni contact was used for the n-type contact. A p-type Ni/Ti/Au contact was used for the back surface.

Cells were isolated by mesa etching to a depth of 2.2 μm in HCl : HNO₃ : DI (1:1:10) at a rate of approximately 80 Å/s. The resultant cells have an area of 0.185 cm².

2.2. Device characterization

The light response measurement (Fig. 2) consisted of a Xenon lamp with an AM1.5 filter at concentration of 1 sun, verified by a silicon cell. The dark current is measured on the same setup as the light current. The internal quantum efficiency (IQE) is measured by filtering the Xenon lamp through a monochromator, measuring the short circuit current per wavelength, and correcting for reflection and absorption. The spectrum power was measured with a thermopile optical power meter.

^{*} Corresponding author. Tel.: +1 765 714 4845.

E-mail address: jjeon@ecn.purdue.edu (J.-H. Jeon).

n-GaP,	1E20, 10 nm
n-GaP,	1E18, 0.5 μ m (Si)
p-GaP,	1E17, 4.5 μ m
p-GaP buffer,	1E18, 0.2 μ m (Be)
p-GaP Substrate,	1E18 (Zn)

Fig. 1. Structure of the baseline GaP photovoltaic cell.

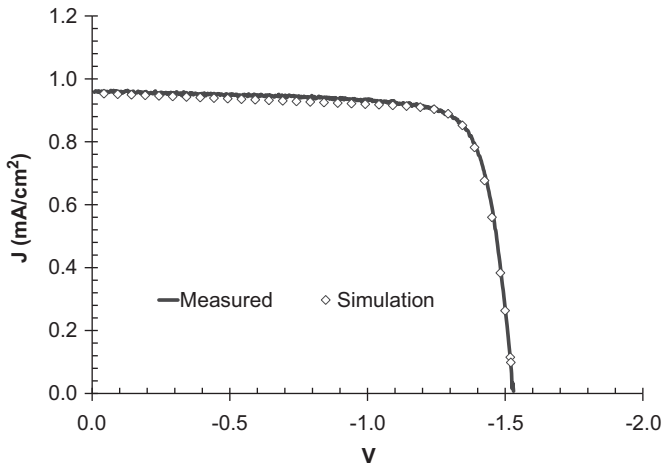


Fig. 2. AM1.5 response of the GaP cell. $V_{oc} = 1.53$ V $J_{sc} = 0.96$ mA/cm².

2.3. Device simulation

To assist in device design, device simulation was conducted using a drift-diffusion based solar cell simulator, ADEPT-F [7]. Curve fitting was accomplished by starting with an assumed ideal device, and logically modifying various parameters to account for likely non-idealities.

3. Results

The n-type contact had a contact resistance of $6 \times 10^{-4} \Omega \text{cm}^2$ after annealing. The p-type contact had a contact resistance of $\approx 1 \Omega \text{cm}^2$. Further investigation is needed to improve the p-type contacts.

The summary of the light response can be seen in Table 1. The light response curve can be seen in Fig. 2. There was no anti-reflective (AR) coating on the cell. The dark response curve can be seen in Fig. 4. The internal quantum efficiency (IQE) can be seen in Fig. 3.

The best fit parameters can be found in Table 2 where d is the layer thickness, ND or NA is the doping concentration, τ_{srh} is the minority carrier lifetime due to Shockley-Read-Hall recombination, and μ is the minority carrier mobility.

3.1. Comparison to state of the art

The idealized 20 suns simulation, extrapolated from the 1 sun model, can be dropped into the 6-junction stack designed by Barnett et al. [8] in place of the 2.4 eV cell. Their ideal target

Table 1
Measured AM1.5 light response.

V_{oc} (V)	J_{sc} (mA/cm ²)	FF	Efficiency
1.53	0.959	0.8	1.17%

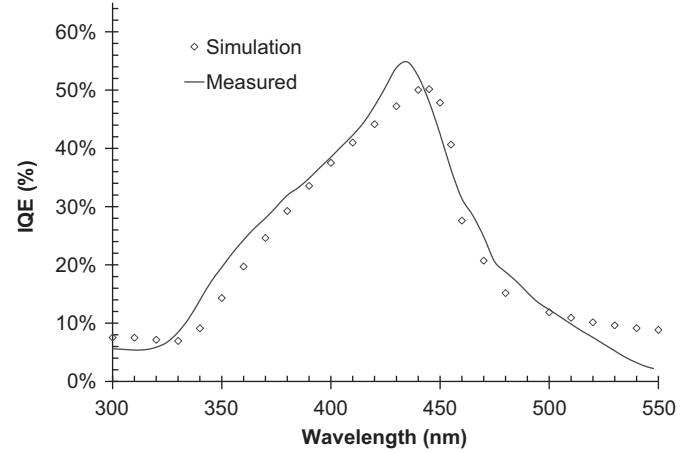


Fig. 3. Internal quantum efficiency of GaP cell.

Table 2
Best fit parameters.

Layer	d	ND or NA (cm ⁻³)	τ_{srh} (s)	μ (cm ² /Vs)
n contact	150 Å	1×10^{19}	6×10^{-12}	78
n active	0.5 μ m	$2.1 \times 10^{18} \rightarrow 0.7 \times 10^{18}$	12.57×10^{-6}	72 \rightarrow 125
p active	4.5 μ m	$0.73 \times 10^{18} \rightarrow 1 \times 10^{18}$	118.4×10^{-12}	64 \rightarrow 59
p buffer	1 μ m	2×10^{18}	1×10^{-12}	66
Series resistance	60 Ω			
Shunt resistance	40 k Ω			
$\chi_s - \Phi_m$	0.2 eV			

efficiency is 13.3% for the highest energy 2.4 eV cell. The simulated ideal GaP cell achieves 12.2% efficiency at $20\times$ concentration without the use of a DBR. The limiting efficiency for single-junction GaP predicted by Henry [1] is approximately 15%. This drop from the ideal efficiency is partially due to the lack of absorption of most of the photons of energies between the direct and indirect band (2.78 and 2.26 eV, respectively) in the 5 μ m GaP active region. If the photons between the direct and indirect bandgaps were reflected back into the GaP, the resulting efficiency can be expected to reach 14%, as seen in Table 4. For the purpose of this evaluation, we will assume the photons not absorbed on the first pass through the GaP are allowed to pass through to lower bandgap cells.

$$\eta_{bot} = \frac{\int_{2.26}^{2.4} \Phi(E)(1 - e^{-\alpha_{GaP}(E)5 \mu m}) dE}{\int_{0.7}^{2.4} \Phi(E) dE} \quad (1)$$

$$\eta_{tot} = \eta_{top}\eta_1 + \eta_{bot} \sum_{i=2}^6 \eta_i \quad (2)$$

To obtain a theoretical value for the maximum efficiency, we can make two observations. The first observation is that the 5 μ m GaP cell is 1.1% less efficient than the optimal 2.4 eV cell over the whole AM1.5 spectrum. The second observation is that the spectrum available to the lower cells is reduced by 1.42%. Eq. (1) expresses this where $\Phi(E)$ is the AM1.5 spectral irradiance as a function of energy. If we let η_i be the ideal target efficiency of each

of the 6 cells in [8], and $\eta_{\text{target}} = \sum \eta_i$, Eq. (2) represents an estimate of the expected efficiency of the stack substituting a GaP cell for the optimal 2.4 eV cell. Compared to the ideal target, we can reduce the top cell's efficiency by a factor of η_{top} , which is the fraction of a GaP cell's efficiency to the ideal top cell efficiency. Since the mid and low energy cells have a different spectrum compared to the optimized 2.4 eV case, a factor of η_{bot} , which is the fraction of the spectrum available to the lower cells compared to the ideal case, can be employed. The most notable changes would be to the mid-gap cells. η_{bot} assumes all necessary adjustments for optimization to the GaP filtered spectrum do not reduce the sum of the bottom cells' efficiencies by more than η_{bot} . The results are summarized in Table 3.

4. Discussion

The best-fit simulation is helpful in revealing limiting flaws in the cell. The IQE measurement gives a good indication of problem areas in the cell. Problems in the short wavelengths are indicative of either front surface or n-type material quality issues. Problems in the longer wavelengths are indicative of either rear surface or p-type material quality issues. The threshold of "long" and "short" wavelengths for GaP are the direct band edge at about 2.76 eV (approx. 450 nm) the indirect band edge at 2.26 eV (approx. 550 nm).

Best-fit simulation parameters can be found by assuming the short wavelength response is limited by surface recombination, and the long wavelength response is limited by minority carrier diffusion lengths in the p-type region. This does not account for all of non-idealities in the device. The energy band diagram best fit for the front surface can be seen in Fig. 5. All minority carriers generated within the front surface drift field are assumed lost.

Another parameter that differs from the ideal is the doping concentration as a function of position. The best-fit parameters vary the doping throughout the device, with the lower concentrations for each active region being closest to the junction. This has the effect of increasing the collection efficiency by inducing drift fields, while lowering V_{oc} due to the lower average doping in the active regions. The best fit doping profile linearly varies from $ND = 2.1 \times 10^{18}$ to $ND = 0.7 \times 10^{18}$ in the n-type active region, and $NA = 0.73 \times 10^{18}$ to $NA = 1 \times 10^{18}$ in the p-type active region. This doping grading augments the diffusion length in the p-type active region, allowing more collection than would otherwise be possible.

Table 3
Estimating GaP stack efficiency.

η_{target}	$\sum_{i=2}^6 \eta_i$	η_{top}	η_{bot}	η_{tot}
53.5%	40.4%	91.7%	98.6%	51.3%

Table 4
Simulation results.

V_{oc} (V)	J_{sc} (mA/cm ²)	Conc.	$\eta_{\text{AM1.5g}}$ (%)	Condition
1.53	0.959	1 ^a	1.2	No AR
1.57	1.96	1	2.6	With AR, no series or shunt resistance
1.81	5.99	1	10.0	Improved front surface and p-type, with AR, no series or shunt resistance
1.86	120	20	11.8	Improved front surface and p-type, with AR, no series or shunt resistance
1.93	136	20	12.2	Improved front surface and p-type, with AR, no series or shunt resistance, passivating back surface
1.93	156	20	14.0	Improved front surface and p-type, with AR, no series or shunt resistance, passivating DBR on back surface

^a Intensity decreased by 4%.

The mobility plays the largest role in the p-type active region. The mobility largely comes into play in determining the diffusion length of the electrons which affects carrier collection and diffusion current. The other major factor in carrier collection is the minority carrier lifetime. For the p-type active region, the minority carrier lifetime is much poorer than expected [5,2]. Since negligible recombination occurs in the n-type active region, the best-fit lifetime and mobility in said region are of no benefit in analysis.

Taking the measured quantum efficiency of the cell and calculating the expected J_{sc} of AM1.5g yields a value slightly higher than measured on the AM1.5 simulator. This discrepancy is well within reason for purposes of designing improvements to the cell. Table 4 uses AM1.5g reduced by 4% in the best-fit simulation case. This discrepancy suspected to be from shadowing from the device contacts.

The final fitting parameters of consideration are the shunt and series resistance. These parameters control the shape of the light IV curve [9]. Fitting the light response shape yields a best-fit shunt resistance of 40 k Ω and a series resistance of 60 Ω . Optimizing this fitting parameter with the previous ones yields the curves in Figs. 2 and 3.

The curve fitting parameters do not give a unique solution. There may be other configurations of thicknesses, dopings, lifetimes, and mobilities that give a similar fitting. The curve fitting parameters appear to reveal the need for front surface passivation and improvement in the quality of the p-type material.

The predicted dark current response closely matches the data, as seen in Fig. 4. Taking out resistive effects reveals a strong $n = 2$ ideality factor, which is common for wide-bandgap materials. The simulation for the dark response matches well in the region of interest (the corresponding voltages for V_{oc} and max power). The

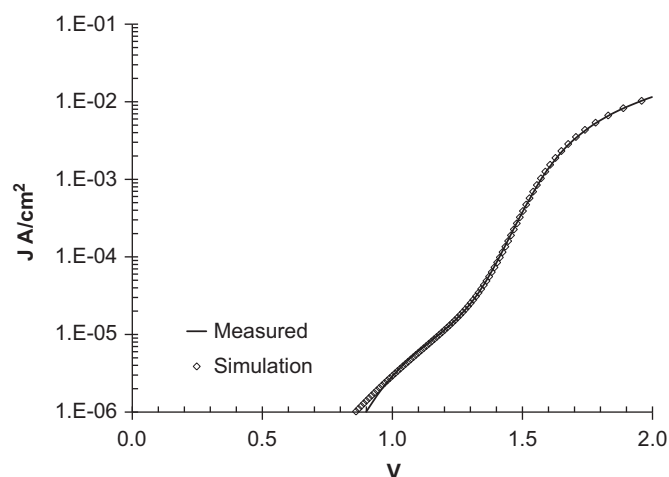


Fig. 4. Dark response of the GaP cell.

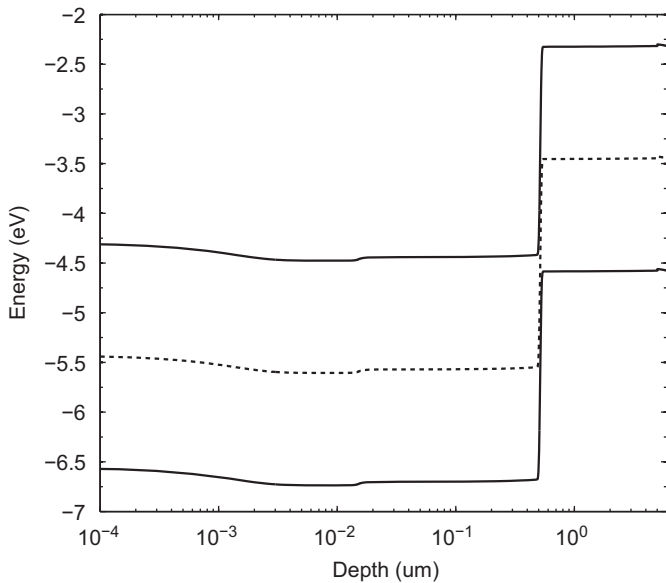


Fig. 5. Energy band simulation of best-fit GaP junction. X-axis is logscale to highlight front surface.

low bias measurement does not match the simulation. Aside from the simulated dark current and effects of series resistance, an extra current is included to fit the lower bias regime in Fig. 4. A rough fit for this extra current can be seen in Eq. (3) where $J_{\text{fit}} = 2.930 \times 10^{-6}$ and $m = 6$. This deviation is believed to be due to effects of traps, which are assumed mid-gap in the simulation. Full investigation of low bias simulation matching is left for future work.

$$J = V * J_{\text{fit}} V^m \quad (3)$$

Taking the simulations a step further where the front surface is passivated by a barrier, and the p-type material growth quality is improved, and a distributed Bragg reflector (DBR) is added to the back surface, expected results are summarized in Table 4. Improvements in carrier collection (front surface passivation, p-type lifetime improvement, and rear surface passivation) have the largest effect on the overall efficiency.

5. Conclusion

Simulation has yielded good insight to the limiting characteristics of a GaP solar cell. Fitting shunt resistance, series resistance, doping profile, and material lifetime has yielded good agreement with laboratory results. A V_{oc} of 1.53 V and a J_{sc} of 0.959 mA/cm² were successfully demonstrated and matched in simulation. Front surface recombination and p-type material quality are believed to be the limiting factors in improving cell efficiency.

To improve front surface characteristics, heterojunction caps have been used on similar materials [10]. AlGaP forms a Type II heterojunction with GaP, making it ideal for use as a hole blocker. High quality ZnS has been grown on GaP [11] and provides another option for front surface passivation.

To improve the p-type material, a superlattice diffusion barrier [12] consisting of AlGaP-GaP layers is being investigated for use between the substrate and the epi-layer. This superlattice can also be tuned as a DBR to only reflect the photons of energies between the direct and indirect band gap.

Fixing the issues in the GaP cell can help lead to multi-junction stack efficiencies of greater than 50%.

Acknowledgments

Thanks to Richard Schwartz and Jeff Gray for assistance in solar cell simulation. Thanks to Hugh Hillhouse for use of his AM1.5 simulator.

References

- [1] C.H. Henry, Limiting efficiencies of ideal single and multiple energy gap terrestrial solar cells, *Journal of Applied Physics* 51 (1980) 4494–4500.
- [2] M. Young, D. Wight, Concentration dependence of the minority carrier diffusion length and lifetime in GaP, *Journal of Physics D: Applied Physics* 7 (1974) 1824–1837.
- [3] S. A. Ringel, Optimized III–V multijunction concentrator solar cells on patterned Si and Ge substrates: final technical report, 15 September 2004–30 September 2006, Final Technical Report NREL/SR-520-44250, NREL, November 2008.
- [4] P.T. Landsberg, *Recombination in Semiconductors*, Cambridge University Press, Cambridge, 1991.
- [5] S. Adachi, *Properties of Group-IV, III–V, and II–VI Semiconductors*, John Wiley & Sons, Ltd, West Sussex, England, 2005.
- [6] O. Sulima, P. Sims, J. Cox, M. Mauk, R. Mueller, R.C. Reedy Jr., A. Khamadov, P. Paulson, G. Landis, High-temperature AlGaP/GaP solar cells for NASA space missions, in: *Proceedings of Third World Conference on Photovoltaic Energy Conversion*, 2003, p. 737.
- [7] J. L. Gray, ADEPT: a general purpose numerical device simulator for modeling solar cells in one-, two-, and three-dimensions, in: *Conference Record of the 22nd IEEE Photovoltaic Specialists Conference*, Las Vegas, Nevada, 1991, pp. 436–438.
- [8] A. Barnett, D. Kirkpatrick, C. Honsberg1, D. Moore, M. Wanlass, K. Emery, R. Schwartz, D. Carlson, S. Bowden, D. Aiken, A. Gray, S. Kurtz, L. Kazmerski, T. Moriarty, M. Steiner, J. Gray, T. Davenport, R. Buelow, L. Takacs, N. Shatz, J. Bortz, O. Jani1, K. Goossen, F. Kiamilev, A. Doolittle1, I. Ferguson1, B. Unger, G. Schmidt, E. Christensen, D. Salzman, Milestones toward 50% efficient solar cell modules, in: *Proceedings of the 22nd EU PVSEC, European Photovoltaic Solar Energy Conference and Exhibition*, 2007, p. 95.
- [9] J. Nelson, *The Physics of Solar Cells*, Imperial College Press, Covent Garden, London, UK, 2003.
- [10] J.M. Woodall, H.J. Hovel, High-efficiency GaAlAs–GaAs solar cells, *Applied Physics Letters* 21 (1972) 379.
- [11] A.N. Krasnov, H.E. Ruda, L. Jedral, L. Mannik, Photo-assisted chemical transport reaction growth of ZnS on GaP, *Journal of Materials Science Letters* 16 (1997) 1167.
- [12] H. Alawadhi, R. Vogelgesang, A.K. Ramdas, T.P. Chin, J.M. Woodall, Indirect transitions, free and impurity-bound excitons in gallium phosphide: a revisit with modulation and photoluminescence spectroscopy, *Journal of Applied Physics* 82 (1997) 4331–4337.